# Dispersion Characteristics in Disk-on-Pillar Array Nanostructures for Surface-Enhanced Raman Spectroscopy

**ARTICLE** *in* THE JOURNAL OF PHYSICAL CHEMISTRY C · JUNE 2011

Impact Factor: 4.77 · DOI: 10.1021/jp2032059

THE JOURNAL OF PHYSICAL CHEMISTRY C

ARTICLE

pubs.acs.org/JPCC

# Dispersion Characteristics in Disk-on-Pillar Array Nanostructures for Surface-Enhanced Raman Spectroscopy

Alessia Polemi,[†] Sabrina M. Wells,[‡] Nickolay V. Lavrik,[§] Michael J. Sepaniak,[‡] and Kevin L. Shuford*[,†]

[†]Department of Chemistry, Drexel University, Philadelphia, Pennsylvania 19104, United States

[‡]Department of Chemistry, University of Tennessee, Knoxville, Tennessee 37996, United States

[§]Center for Nanophase Materials Sciences, Oak Ridge National Laboratory, Oak Ridge, Tennessee 37831, United States

**ABSTRACT:** In this paper, we analyze periodic disk-on-pillar nanoarrays as a platform for surface-enhanced Raman spectroscopy measurements. The nanostructure is a two-dimensional grating of silicon pillars covered by thin layers of silica and silver. The system supports both localized surface plasmons and surface plasmon polaritons. We investigate the dispersion characteristics of the nanoarray and present the relevant field distribution for each plasmon mode. The interaction between localized and propagating modes can be tuned to synergistically enhance the electric field, which results in larger surface-enhanced Raman signals. We find that utilizing this effect can generate Raman enhancements that are approximately 1000 times larger than that of an isolated pillar under the same excitation conditions.

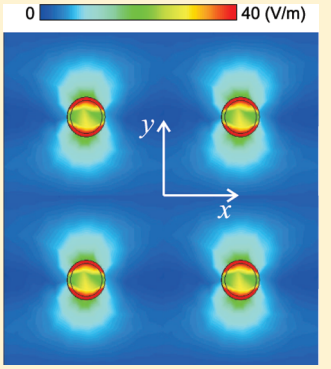


## INTRODUCTION

There has been a renewed interest in surface-enhanced Raman spectroscopy (SERS) in the past decade, as both nanostructure fabrication methods and analytical measurement techniques have improved substantially. SERS is a powerful technique for sensing trace amounts of a given analyte and in some cases permits the detection of single molecules.[1,2] The SERS effect is largely based on sizable electromagnetic fields near metal surfaces resulting from the excitation of localized surface plasmons (LSPs). Although chemical mechanisms do occur in SERS, the electromagnetic contribution is believed to dominate the signal enhancement.[3,4] Excitation of strong plasmonic resonances can be achieved in individual nanoparticles, such as colloids, as well as via coupling to adjacent interfacial features like roughened surfaces. However, the need for signal reproducibility has driven recent fabrication trends toward regular gratings, where surface features are well-defined. That is, the properties of the metals, the dielectric environment, the morphology of the nanoparticles, and their interspacing are known.[5,6]

Recently, a fabrication scheme has been developed that can produce high-quality pillar nanostructures for SERS measurements.[7−9] The surface is obtained through a sequence that involves electron beam lithography, anisotropic reactive ion etching of Si, plasma-enhanced chemical vapor deposition of $SiO_2$, and physical vapor deposition of Ag. The resulting nanoelement is a Si pillar that supports a larger diameter, disk nanoparticle composed of a layer of $SiO_2$ followed by a layer of Ag. We call this nanoelement disk-on-pillar (DOP). The DOP element resides on a Si substrate, which is also covered by a double layer of $SiO_2$ and Ag. The electromagnetic phenomenology associated with a single DOP has been investigated previously.[10] This study carefully examined how variations in the DOP morphology altered the local electric field distribution.

The DOP geometry can also be fabricated in an array format. When arranged in a periodic configuration, the nanoelements provide a stronger enhancement of the local field due to the interaction between multiple resonances. The DOP nanostructure supports a LSP of the Ag nanodisk, while the Ag surface supports surface plasmon polaritons (SPPs). These two resonance frequencies are typically quite different; however, the presence of a grating creates periodicity induced SPPs, also called Floquet wave (FW) induced SPPs. Their periodic spectral replica can fall close to the LSP resonance creating a strong plasmonic coupling. This coupling is responsible for highly uniform field hot spots along the array. Assuming an infinite array, the spectral momentum associated with the FW-induced SPPs is controlled by the geometric characteristic of the periodic unit cell.

In this paper, we investigate the dispersion properties of the DOP nanostructure, with particular emphasis on the plasmonic interaction between LSPs and FW-induced SPPs. Since we are interested in SERS, we examine how the DOP dispersion properties influence the SERS enhancement, which is assumed to scale as the fourth power of the electric field averaged over the surface of the nanodisk. We have already observed that this figure of merit is less sensitive to numerical issues, such as the size of the

**Received:** April 6, 2011
**Revised:** June 8, 2011
**Published:** June 13, 2011

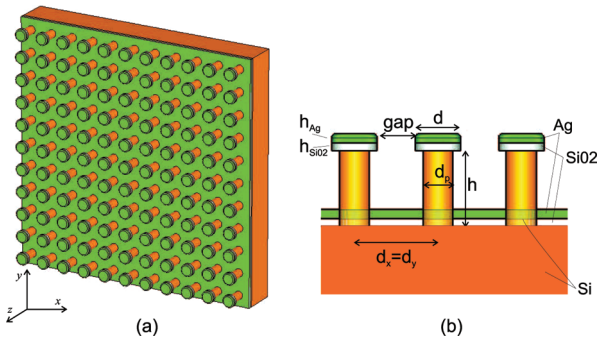


**Figure 1.** Geometry of the infinite DOP nanoarray. (a) 3D view. (b) Side view and geometrical parameters.

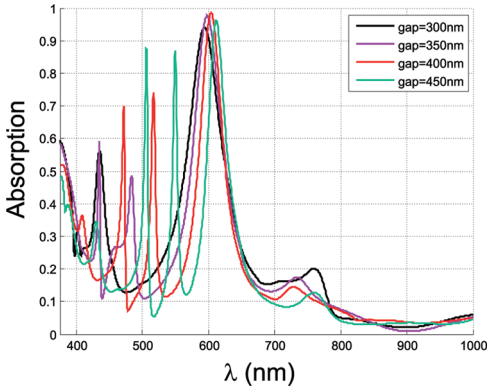


**Figure 2.** Absorption of the DOP array for different values of the gap distance. The pillar height is $h$ = 90 nm, and the pillar and disk diameters are $d_p$ = 80 nm and $d$ = 120 nm, respectively.

mesh cell in the model.[10] We show here that the resulting electric field is directly related to the coupling between LSPs and FW-induced SPPs, and the structural parameters of the nanoarray can be adjusted to exploit the interaction resulting in larger SERS enhancements.

## METHODOLOGY

Figure 1 shows the system under investigation. The nanostructure is composed of DOP nanoelements regularly displaced in an infinite array configuration as shown in Figure 1a. The geometry of an individual DOP element is identical to those studied previously.[10] A detailed view on the array including the geometrical parameters is shown in Figure 1b. The pillar is modeled as a Si rod with diameter $d_p$ and height $h$ and resides on a macroscopic Si slab (assumed infinite). A thin $SiO_2$ layer ($h_{SiO_2}$ = 20 nm) covers the Si slab and the top of the pillar with refractive index $n_{SiO_2}$ = 1.45. The Ag layer has a height $h_{Ag}$ = 25 nm. Ag and Si dispersion has been incorporated via experimentally determined values of the optical constants.[11] The Ag disks have diameter $d$, and they are uniformly separated by the distance *gap* making the array unit cell $d_x = d_y = gap + d$. The top edge of the Ag disks have been rounded to better approximate the real fabricated pillar.[9]

The structure has been analyzed numerically using a full wave method based on the finite difference technique[12] implemented in CST Microwave Studio.[13] The array is assumed infinite in both the $x$ and $y$ directions so unit cell boundary conditions can be

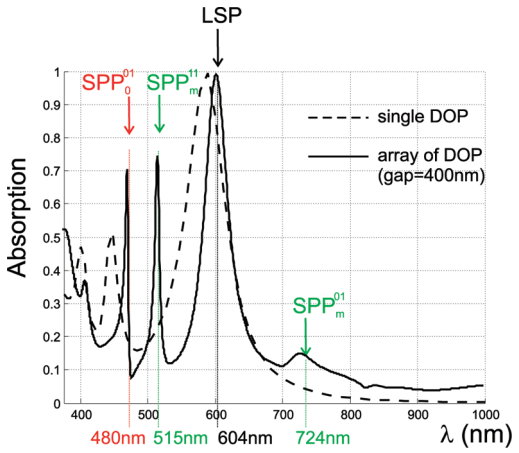


**Figure 3.** Absorption of an array of DOP elements separated by distance *gap* = 400 nm (solid line). The absorption of a single DOP is also shown (dashed line).

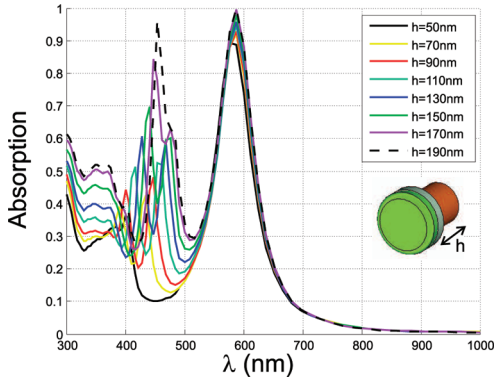


**Figure 4.** Absorption of a single DOP nanoelement for different values of the pillar height $h$.

applied. The structure has been meshed with tetrahedrons and analyzed in the frequency domain. A plane wave impinges normally on the structure (direction $-z$ in Figure 1a). We assume a linear polarization along $y$ (this can be easily extended to the case of different polarizations, such as double linear or circular) and an amplitude of the electric field $E_0 = 1V/m$.

## RESULTS AND DISCUSSION

**Optical Properties of the DOP Nanoarray.** We first analyze the optical response of the DOP array in terms of absorption. The absorption is calculated by means of the reflection and transmission coefficients of the unit cell ($A = 1 - |R|^2 - |T|^2$). In particular, we set the following geometrical parameters: $h$ = 90 nm, $d_p$ = 80 nm, $d$ = 120 nm. The pillar and disk diameters are chosen according to the analysis performed previously for a single DOP element.[10] The absorption is shown in Figure 2 for different values of the gap distance. Several resonances are excited as indicated by numerous absorption peaks at different wavelengths. The resonance around 600 nm is stronger and less affected by the change in the periodicity, while the resonances to the left (shorter wavelengths) vary significantly as the array structure is altered. The dominant resonance at 600 nm corresponds to the LSP associated with the silver disk, which when


dx.doi.org/10.1021/jp2032059 |J. Phys. Chem. C 2011, 115, 13624–13629

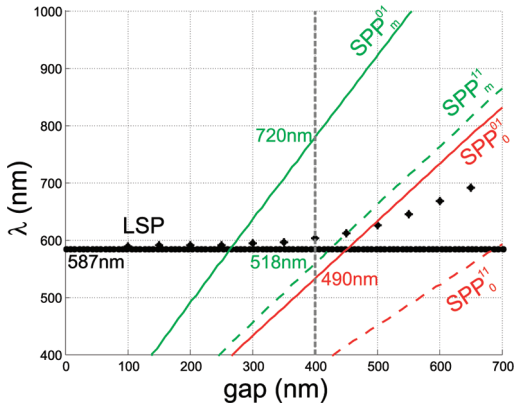


**Figure 5.** Dispersion diagram of the DOP nanoarray. The LSP resonance is shown for the ideal, uncoupled case (black line) and for the real coupled case (dotted black line). The FW-induced SPP dispersion is shown for plasmons propagating at both air−Ag (red lines) and the $SiO_2$−Ag (green lines) interfaces. For both interfaces, we show the first two modes as explained in the text.

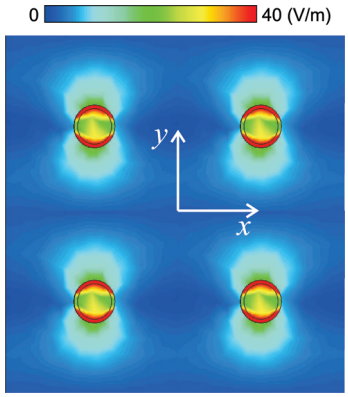


**Figure 6.** Top view. Electric field modulus at the LSP resonance $\lambda$ = 604 nm for the case where *gap* = 400 nm.

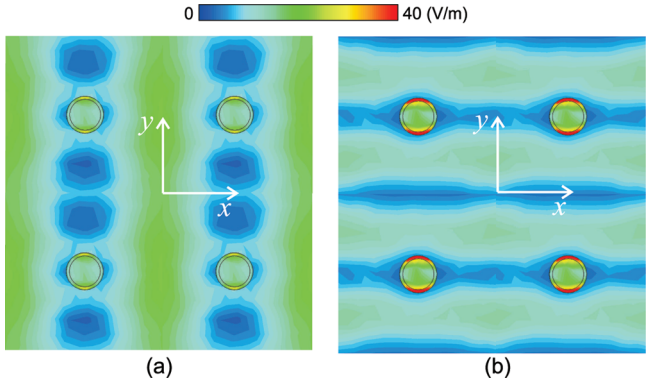


**Figure 7.** Top view. (a) Electric field modulus at the $SPP_m^{11}$ resonance $\lambda$ = 515 nm. (b) Electric field modulus at the $SPP_0^{01}$ resonance $\lambda$ = 480 nm. In both cases, *gap* = 400 nm.

placed in the array configuration tends to red shift with increasing gap distance.

To analyze the resonance phenomena in detail, we focus on the case where *gap* = 400 nm. The absorption is plotted in Figure 3 as a solid line for the array, and the absorption of a single DOP, formed only by the nanodisk and the pillar, is shown as a dashed line. For the single DOP, we have intentionally removed the surface to focus on the effect of the pillar and eliminate all other couplings. It can be seen that the LSP resonance slightly red shifts when other DOP nanoelements are present (604 nm in the array configuration, 587 nm in the single element configuration). We note from the single DOP case an increase of absorption at 400 and 450 nm resulting from absorption of the Si pillar. The influence of pillar size on this spectral region is plotted separately in Figure 4, where the absorption of the single DOP is shown for different pillar heights *h*. While the LSP resonance at 600 nm does not change, the Si absorption becomes more intense and red shifts as the pillar height is increased. This indicates that the absorption below 500 nm results primarily from the Si pillar in the absence of surface or array couplings.

Returning to the array case in Figure 3, there are multiple peaks that are not present in the single DOP spectrum and therefore do not originate from the individual Si pillars. These resonances are generated by FW-induced SPPs. The air−Ag and $SiO_2$−Ag interfaces support SPPs according to the well-known formula[14]

$$k_{SPP} = k\sqrt{\frac{\varepsilon_1\varepsilon_2}{\varepsilon_1 + \varepsilon_2}} \quad (1)$$

where $k_{SPP}$ is the SPP wavenumber, $k = 2\pi/\lambda$ is the free space wavenumber, and $\varepsilon_1$ and $\varepsilon_2$ are the frequency-dependent permittivities of the materials. This expression reflects a single SPP propagating along the interface of two infinitely thick layers (i.e., no intersurface SPP coupling). Although this is not necessarily the case here, we will utlize eq 1 as a guide to interpret the excitations supported in our more complex nanosurface. When the SPP momentum $k_{SPP}$ couples with the Floquet modes supported by the grating, the in-phase interference gives rise to a diffraction mechanism that generates additional peaks in the absorption spectrum. In particular, this occurs when

$$k_{SPP} = \sqrt{\left(\frac{2\pi p}{d_x}\right)^2 + \left(\frac{2\pi q}{d_y}\right)^2} \quad (2)$$

where $d_x$ and $d_y$ are the interelement spacings along *x* and *y* and *p* and *q* are integers. In our case, $d_{x,y} = gap + d$. Note that there is no additional phasing along *x* and *y* since the plane wave is impinging normally on the interface. Equation 2 can be rewritten using eq 1 into an implicit expression in terms of the wavelength[15,16]

$$(gap + d)\sqrt{\frac{\varepsilon_1\varepsilon_2}{\varepsilon_1 + \varepsilon_2}} = \lambda\sqrt{p^2 + q^2} \quad (3)$$

This last equation can be solved numerically. Here, we have used a standard routine of zeros searching implemented in Matlab.[17] The calculation has been performed for both the air−Ag and the $SiO_2$−Ag interface by varying the number of the FW modes *p* and *q*. Dispersion curves are shown in Figure 5 where $\lambda$ is plotted vs *gap*. The FW-induced SPPs are shown in green for the $SiO_2$−Ag interface (*m* subscript) and in red for the air−Ag interface (0 subscript). The first few modes are displayed, where $p^2 + q^2 = 1$ and $p^2 + q^2 = 2$. The modes have 4-fold degeneracy, since $p^2 + q^2 = 1$ occurs for indices $p = 0$, $q = \pm 1$ and $p = \pm 1$, $q = 0$, while the condition $p^2 + q^2 = 2$ occurs when

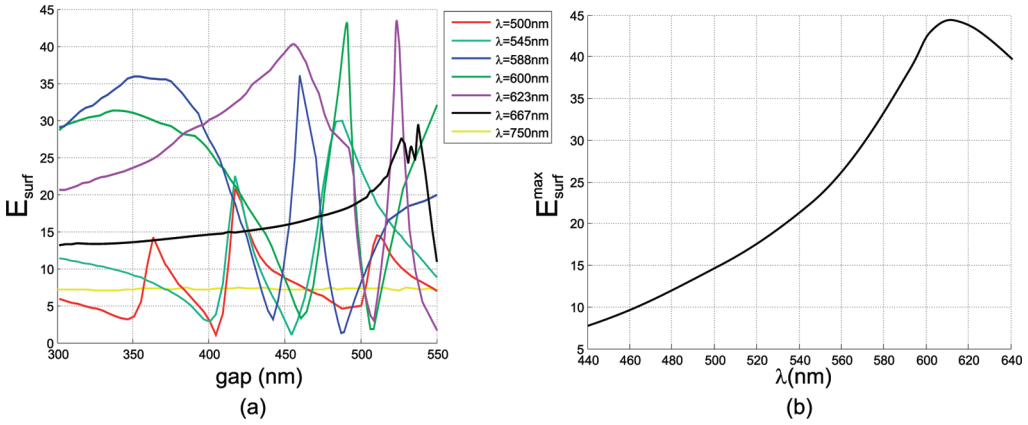


**Figure 8.** (a) Total absolute field integrated over the disk surfaces as a function of the gap distance for different wavelengths. (b) The maxima of $E_{surf}$ across the span of gap values plotted vs incident wavelength. The global maximum is ~45 and occurs at $\lambda \approx 610$ nm.

$p = \pm 1, q = \pm 1$. Since the incident electric field is polarized along $y$, we assume that the primary coupling occurs along $y$. Thus, for the condition $p^2 + q^2 = 1$, the leading mode is considered $p = 0$, $q = 1$. Specific SPP resonances for the case of an array with *gap* = 400 nm are shown in Figure 5, and the corresponding wavelengths reasonably approximate the resonances $SPP_0^{01}$, $SPP_m^{01}$, and $SPP_m^{11}$ denoted in Figure 3. The LSP dispersion is also plotted in black. The horizontal line at 587 nm is the LSP of the silver disk, which theoretically does not depend on the periodicity. Practically, when inserted into the array configuration, the LSP resonance also undergoes a small dispersion, as shown by the black dots in Figure 5. The effect is larger at wavelengths when the LSP resonance approaches that of the SPPs. This analysis shows that the absorption spectrum can be attributed to two main mechanisms: the LSP resonance associated with the Ag disk and the SPP resonances, which are induced by the grating (Floquet modes).

**LSP and SPP Field Distribution.** In this subsection, we show the electric field at the resonance frequencies of the LSP and of the two dominant FW-induced SPPs. For the LSP resonance, the main absorption is due to the Ag disk on top of the DOP nanoelement, while for the FW-induced SPPs, the field is concentrated primarily around the base of the pillar. We present the case where *gap* = 400 nm, and the periodicity is $d_x = d_y =$ 520 nm. Figure 6 shows the modulus of the electric field for the LSP resonance, where the field is localized and most intense around the elevated disk. The field pattern centered on each pillar is consistent with a dipole excitation of a disk-shaped nanoparticle. Figure 7 shows the electric field for the $SPP_m^{11}$ mode and the $SPP_0^{01}$ in panels a and b, respectively. The field pattern for the $SPP_m^{01}$ mode is not plotted but is very similar to the $SPP_0^{01}$ mode. Note that the SPP fields are less intense than the LSP field, as expected from the relative intensities in the absorption spectrum (Figure 3). Also, Figure 7 reveals the pattern dictated by indices of the propagating modes. The indices $p = 1$, $q = 1$ are associated with a mode with wavefronts traveling both along $x$ and $y$, while the mode with indices $p = 0$, $q = 1$ has a wavefront primarily traveling along $y$. These mode properties can be clearly observed in Figure 7.

**Dispersion of SERS Gain.** For SERS applications, we want to maximize the field around the nanoparticle, quantified here as a gain factor $G$. There are different ways to define the SERS enhancement factor $G$ of this structure.[16,18,19] We assume that $G$ is proportional to the fourth power of the local electric field.[20] The local field around the nanoparticle spikes in the proximity of its edges, so we define a more representative figure of merit by averaging the electric field over the surface area as was done previously.[10] In particular, we define $E_{surf}$ as the total absolute field integrated over the surfaces of the disk ($S_{disk}$) accessible to molecules

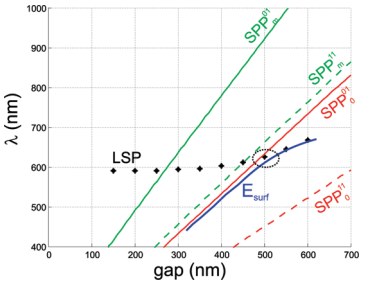


**Figure 9.** Dispersion diagram including the dispersion of $E_{surf}$ (blue line). The maximum field enhancement is attained when the LSP resonates with the SPPs supported by the periodic structure, as indicated by the dotted circle.

$$E_{surf} = \frac{1}{S_{disk}} \int_{S_{disk}} |\vec{E}(x,y,z)| dS \qquad (4)$$

In this way, the enhancement factor can be expressed as $G = E_{surf}^4$.

In Figure 8a, we show $E_{surf}$ as a function of the gap distance for different excitation wavelengths. This plot shows the maxima shift with frequency. In Figure 8b, we plot the largest value of $E_{surf}$ as a function of wavelength. The global maximum reaches ~45 at excitation wavelength $\lambda \approx 610$ nm, which corresponds to $G = 4 \times 10^6$. This value compares favorably with other SERS substrates, especially considering that we calculate $G$ using the surface averaged electric field, which will be considerably less than the maximum value. It is evident that $E_{surf}$ undergoes a dispersion, which is better displayed in Figure 9, where the dispersion diagram is shown upon adding the dispersion curve related to the largest value of $E_{surf}$ for a range of excitation wavelengths (blue line). The strongest field enhancement is attained at approximately 610 nm for a 494-nm gap distance, where the LSP resonates with the FW-induced $SPP_0^{01}$ (denoted by dotted circle). For small gap distances between the DOP


dx.doi.org/10.1021/jp2032059 |J. Phys. Chem. C 2011, 115, 13624–13629

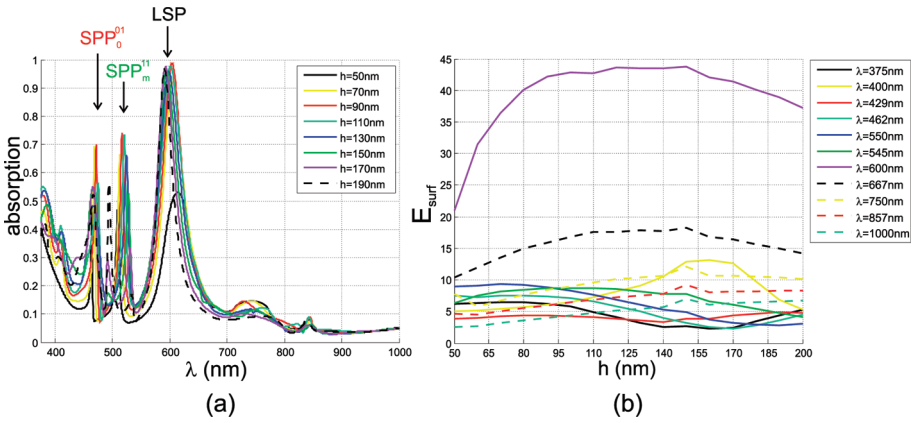


**Figure 10.** (a) Absorption spectra of the DOP nanosurface for different values of the pillar height $h$. (b) Variation of $E_{surf}$ in terms of the pillar height $h$ for multiple values of wavelength. The gap distance is 494 nm.

nanoparticles (but large enough that there is no LSP coupling), the $E_{surf}$ dispersion is dominated by the SPP since the structure is strongly coupled. When the gap distance is greater than ~550 nm, the DOP nanoparticles are well separated, and the uncoupled LSP resonance dominates the resulting surface field. In fact, the $E_{surf}$ curve closely tracks the LSP dispersion in this regime. For a gap = 1 $\mu$m and $\lambda$ = 610 nm (not shown in the figure), $E_{surf} \approx 8$, which yields $G = 4 \times 10^3$. At this spacing, the surface field should originate almost exclusively from the LSP resonance, which suggests that the optimized structure described above produces an additional $10^3$ SERS enhancement from SPP coupling. The primary source and magnitude of the field enhancement is an important aspect to consider for the design and optimization of periodic SERS surfaces, especially those that operate at a fixed frequency. Experimental verification of these findings are underway currently and will be presented in a later publication.

**Dependence on Pillar Height.** Figure 10a shows the absorption spectra of the DOP nanosurface for different values of the pillar height $h$. As anticipated from Figure 4, the size of the pillar changes the absorption of the structure due to amount of Si present. The LSP and SPP resonances are almost unvaried, while new resonances appear at shorter wavelengths as shown in Figure 10a and discussed previously with respect to Figure 4. In Figure 10b, we show the variation of $E_{surf}$ in terms of the pillar height for multiple values of the incident wavelength. As noted above, the wavelength at which the field enhancement is maximized corresponds to values close to 600 nm as is clearly observed in the figure. Furthermore, Figure 10b further shows that the field enhancement at a particular incident wavelength is not strongly dependent upon the pillar height, at least for the range of values between 80 and 180 nm, where the value of $E_{surf}$ undergoes only a small variation. As such, the optical properties of DOP nanoarrays are less sensitive to potential fabrication issues, which is extremely desirable for systems where SERS measurements are performed.

## CONCLUSIONS

In this paper, we have investigated how the DOP nanoelement in an array configuration can be used for SERS. The nanostructure is composed of a two-dimensional grating of silicon pillars, with a double layer of $SiO_2$ and Ag on top of the pillars as well as lining the Si substrate. The nanosurface supports both localized surface plasmons and surface plasmon polaritons. The dispersion characteristics of the LSP and SPP modes and their relevant field distributions have been presented and discussed. We have shown that the interaction between these two kinds of resonances can be used to increase the SERS enhancement factor considerably. Moreover, once optimized, DOP nanoarrays are relatively insensitive to small fluctuations in pillar height or spacing, ultimately making these nanostructures more robust sensing platforms.

## AUTHOR INFORMATION

### Corresponding Author

*E-mail: shuford@drexel.edu.

## ACKNOWLEDGMENT

A portion of this research was conducted at the Center for Nanophase Materials Sciences, which is sponsored at Oak Ridge National Laboratory by the Division of Scientific User Facilities, U.S. Department of Energy. K.L.S. thanks Drexel University for start-up funding.

## REFERENCES

(1) Nie, S.; Emory, S. R. *Science* **1997**, *275*, 1102–1106.
(2) Kneipp, K.; Wang, Y.; Kneipp, H.; Perelman, L. T.; Itzkan, I.; Dasari, R. R.; Feld, M. S. *Phys. Rev. Lett.* **1997**, *78*, 1667–1670.
(3) Kim, H.; Cheng, X. *Opt. Express* **2009**, *17*, 17234–17241.
(4) Banholzer, M. J.; Millstone, J. E.; Qin, L.; Mirkin, C. A. *Chem. Soc. Rev.* **2008**, *37*, 885–897.
(5) Genov, D. A.; Sarychev, A. K.; Shalaev, V. M.; Wei, A. *Nano Lett.* **2004**, *4*, 153–158.
(6) Gantzounis, G.; Stefanou, N.; Papanikolaou, N. *Phys. Rev. B* **2008**, *77*, 035101–035108.
(7) Wells, S. M.; Retterer, S. D.; Oran, J. M.; Sepaniak, M. J. *ACS Nano* **2009**, *3*, 3845–3853.
(8) Bhandari, D.; Wells, S. M.; Retterer, S. T.; Sepaniak, M. J. *Anal. Chem.* **2009**, *81*, 1456–1466.
(9) Wells, S. M.; Polemi, A.; Lavrik, N. V.; Shuford, K. L.; Sepaniak, M. J. *Chem. Commun.* **2011**, *47*, 3814–3816.
(10) Polemi, A.; Wells, S. M.; Lavrik, N. V.; Sepaniak, M. J.; Shuford, K. L. *J. Phys. Chem. C* **2010**, *114*, 18096–18102.
(11) Palik, E. *Handbook of Optical Constants of Solids*, 1st ed.; Academic Press: Orlando, 1985.
(12) Weiland, T. *Electron. Commun.* **1977**, *31*, 116–120.

(13) www.cst.com, 2010.
(14) Raether, H. *Surface Plasmons on Smooth and Rough Surfaces and on Gratings*, 1st ed.; Springer-Verlag: Berlin, 1988.
(15) Ghaemi, H.; Thio, T.; Grupp, D.; Ebbesen, T.; Lezec, H. *Phys. Rev. B* **1998**, *58*, 6779–6782.
(16) Montgomery, J.; Imre, A.; Welp, U.; Vlasko-Vlasov, V.; Gray, S. K. *Opt. Express* **2009**, *17*, 8669–8675.
(17) www.mathworks.com.
(18) Beermann, J.; Novikov, S. M.; Leosson, K.; Bozhevolnyi, S. I. *Opt. Express* **2009**, *17*, 12698–12705.
(19) Knorr, I.; Christou, K.; Meinertz, J.; Selle, A.; Ihlemann, J.; Marowsky, G. *Proceedings COMSOL Conference*, 2008.
(20) Kahl, M.; Voges, E. *Phys. Rev. B* **2000**, *61*, 14078–14088.